Nanostructured Catalysts

DOI: 10.1002/anie.201008013

Nanosizing Intermetallic Compounds Onto Carbon Nanotubes: Active and Selective Hydrogenation Catalysts**

*Lidong Shao, Wei Zhang, Marc Armbrüster, Detre Teschner, Frank Girgsdies, Bingsen Zhang, Olaf Timpe, Matthias Friedrich, Robert Schlögl, and Dang Sheng Su**

Dedicated to the Fritz Haber Institute, Berlin, on the occasion of its 100th anniversary

Recently, much attention has been focused on nanocrystalline intermetallic compounds.[1–4] For instance, current studies of formic acid fuel cells require intermetallic compounds at nanoscale dimensions as anode materials.[5–8] Ideas of using nanoscale intermetallics are based on their modified electronic and structural properties compared with their bulk metallic counterpart. In the case of fuel cells, conventional catalysts, such as platinum, are readily self-poisoned by the CO that is produced as a side-product.[9,10] As for activity, supported intermetallic nanoparticles are necessary to achieve high mass activity and complete resistance to CO poisoning.[8] In the case of Pd-based intermetallics, the unsupported Pd_xGa_y series has been investigated and applied in alkyne-selective hydrogenation.[11–17] It is widely believed that the presence of palladium atom ensembles (continuous neighboring atomic sites) is responsible for full hydrogenation but also causing deactivation.[18,19] Adding Ga can breach Pd atom ensembles and affect their adsorbing abilities. Conventional synthesis of Pd_xGa_y intermetallics requires melting the corresponding amounts of palladium and gallium metals at high temperatures.[11–17] Furthermore, owing to the various stoichiometric ratios of Pd_xGa_y, forming a phase-pure Pd_xGa_y may require further annealing.[16] Therefore, nanosizing and supporting the annealed metal products remain challenges.

Another difficulty is in directly preparing supported catalysts while simultaneously obtaining good crystallite size control. A good catalyst support should be capable of inhibiting sintering and loss of the catalyst during reaction. Fabrication of supported intermetallics catalysts in nanoscale dimensions requires a reliable method that facilitates not only size control but a thermally stable phase under reaction conditions. Since the work of Iijima in 1991,[20] carbon nanotubes (CNTs) have been extensively studied and applied in a wide range of fields owing to their extraordinary physical and chemical properties.[21,22] Aided by their high surface area and one-dimensional hollow structures, CNTs have been utilized in heterogeneous catalysis as supporting materials for anchoring nanoscale metal species on the outside or inside their channels. Dispersed oxidized vacancies[23,24] can be used in bonding nanoparticles to carbon surface. Interactions between metal atoms and localized double bonds on curved CNT[25,26] also permit the formation of nanoparticles.

Herein, we present an impregnation method to fabricate nanocrystalline Pd_2Ga intermetallic on CNTs (Pd_2Ga/CNT) at a low temperature where sintering does not result in particle aggregations. Calcinating the adsorbed metal cations on CNTs and further reducing in H_2 with a controlled ramping rate favor the crystallization of intermetallic Pd_2Ga nanoparticles. We show that subsurface chemistry and carbonaceous deposition are suppressed on nanoscale Pd_2Ga under reaction conditions. In situ results present solid evidence that nanocrystalline Pd_2Ga supported on CNTs are electronically and structurally stable under a reactive atmosphere. Catalytic measurement for Pd_2Ga/CNT was conducted for acetylene hydrogenation and results were compared with the commonly used $Pd_{20}Ag_{80}$ catalyst.

Figure 1a shows XRD patterns of Pd_2Ga supported on CNTs. A homogeneous dispersion of Pd_2Ga nanoparticles on CNTs was observed in STEM mode (Figure 1b). In line with XRD identifications, STEM-EDX analysis and elemental maps of individual nanoparticles on CNTs reveal the homogeneous composition of Pd and Ga in Pd_2Ga nanoparticles (Figure 1c).

Figure 2 shows HRTEM image of a Pd_2Ga nanoparticle supported on CNT together with corresponding Wulff construction.[27,28] Based on the crystal model of Co_2Si type of Pd_2Ga with space group *Pnma*[29,30] of $a = 5.493$, $b = 4.064$, and $c = 7.814$ Å (see the unit cell of Pd_2Ga in Figure 2a), the crystal planes (103) and (−210) were identified with the characteristic acute angle of 69.2°, which is consistent with the HRTEM image simulation of the phase (see the circled area).

Based on the observed information of planes and acute angles, the exposed facets can be identified as {210}, {202}, {020}, {113}, and {103} planes (Figure 2b). On the basis of Wulff constructions, we observed that the exposed facets of most Pd_2Ga particles are terminated by same planes. Using the same way, facets of Pd_2Ga in contact with CNT can also be identified. It can be seen that Pd_2Ga nanoparticles exhibit

[*] Dr. L. Shao, Dr. W. Zhang, Dr. D. Teschner, Dr. F. Girgsdies, Dr. B. Zhang, Dr. O. Timpe, Prof. Dr. R. Schlögl, Dr. D. S. Su
Department of Inorganic Chemistry
Fritz Haber Institute of the Max Planck Society
Faradayweg 4-6, 14195 Berlin (Germany)
Fax: (+49) 30-8413-4401
E-mail: dangsheng@fhi-berlin.mpg.de
Homepage: http://www.fhi-berlin.mpg.de
Dr. M. Armbrüster, M. Friedrich
Max-Planck-Institut für Chemische Physik fester Stoffe
Nöthnitzer Strasse 40, 01187 Dresden (Germany)

[**] The authors acknowledge the support from the EnerChem Project in Fritz Haber Institute of the Max Planck Society.

Supporting information for this article is available on the WWW under http://dx.doi.org/10.1002/anie.201008013.

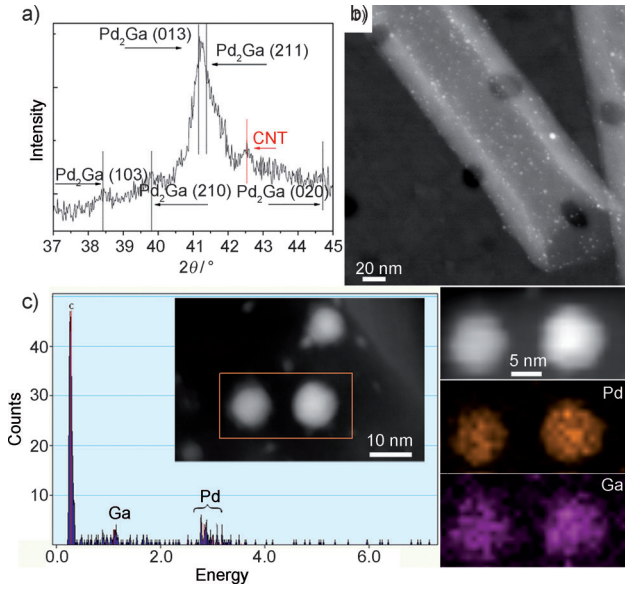

Figure 1. Pd_2Ga Nanoparticles on a carbon nanotube. a) XRD pattern of Pd_2Ga/CNT. b) STEM image of Pd_2Ga supported on CNTs. c) STEM-EDX element mapping of Pd_2Ga particles supported on a CNT. In the microscopy analysis, 15 nm porous silicon films were used to support the sample.

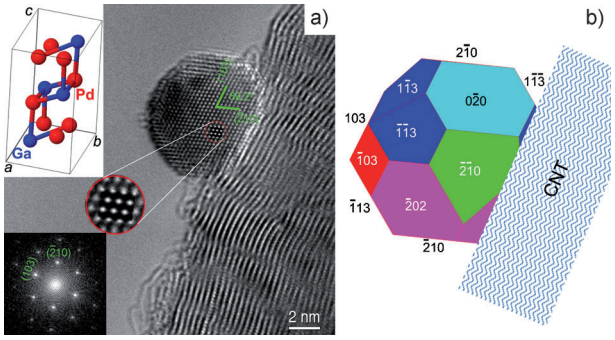

Figure 2. Microstructure characterizations of the Pd_2Ga/CNT. a) HRTEM image, with the insets of (top) crystallographic model of Pd_2Ga and (bottom) the fast Fourier transform of the local HRTEM image. The circled area represents the image simulation, conditioned at defocus of 6 nm and thickness of 6.1 nm viewed along the $\langle -361 \rangle$ direction of Pd_2Ga. b) The Wulff constructions of the corresponding Pd_2Ga nanoparticle in (a).

abundant low coordination sites (edge, stepped, and kink) on surface.

Figure 3 shows Pd_2Ga nanoparticles as small as 2 nm supported on CNTs. The crystal planes and interplanar distances, as well as acute angles, are labeled adjacent to the corresponding Pd_2Ga nanoparticles. The inset shows the size distribution of Pd_2Ga nanoparticles supported on CNTs.

To investigate the surface and surface-near properties of the sample, in situ X-ray photoelectron spectroscopy has been performed under two conditions: before reaction (1.0 mbar of H_2 at 120 °C) and during reaction (0.1 mbar of C_2H_2 mixed with 1.0 mbar of H_2 at 120 °C). XPS measurements for Pd_2Ga/CNT before reaction displayed a significant modification of the palladium electronic states. Referring to reported in situ

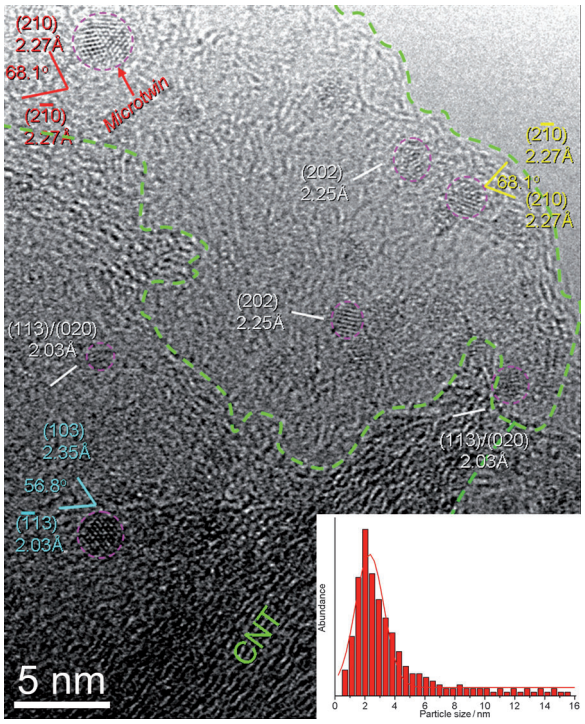

Figure 3. HRTEM image of Pd_2Ga nanoparticles supported on CNT. The mouth of the CNT is outlined by green dashed lines. The clearly-identified nanoparticles are circled by pink dashed-lines. The crystal planes and their interplanar distances, as well as some acute angles, are labeled adjacent to the corresponding nanoparticles. The inset shows the particle size distribution of Pd_2Ga nanoparticles supported on CNT.

XPS studies of Pd catalysts,[31,32] the Pd 3d peak for Pd_2Ga/CNT is shifted by 0.8 eV to higher binding energy (see Figure 4). This observation is consistent with previous studies of PdGa intermetallics,[11] in which filling of the valence d band of Pd was explained by covalent interactions between Pd and Ga. As for the Ga 3d region in Pd_2Ga/CNT before reaction (see Figure 4), oxidation of gallium with binding energies at (20.0 ± 0.1) eV and (21.0 ± 0.1) eV was observed.[33,34] More importantly, a doublet component at 18.5 eV and 19.0 eV corresponding to intermetallic gallium in the Pd_2Ga/CNT, consistent with PdGa,[11] can be detected. Under acetylene hydrogenation conditions, in situ XPS observations of Pd_2Ga/CNT performed at about 1 mbar showed a stable Pd surface with no appearance of new peak or detectable shift of the Pd 3d signal. This observation is in contrast to studies on Pd monometallic catalyst[35] in which an additional PdC_x phase was detected. As for gallium components, relative concentrations remained constant during reactions, which indicates stable gallium oxidation states on the surface under reaction conditions. In situ XPS investigations reveal that surfaces of supported Pd_2Ga intermetallics are electronically stable under applied reaction conditions.

To investigate the structural stability of Pd_2Ga nanoparticles under reactive conditions, in situ XRD was applied. First, an in situ XRD investigation was carried out in H_2 for the observation of Pd β-hydride formation. The XRD study detected no new phase apart from XRD profiles of Pd_2Ga and

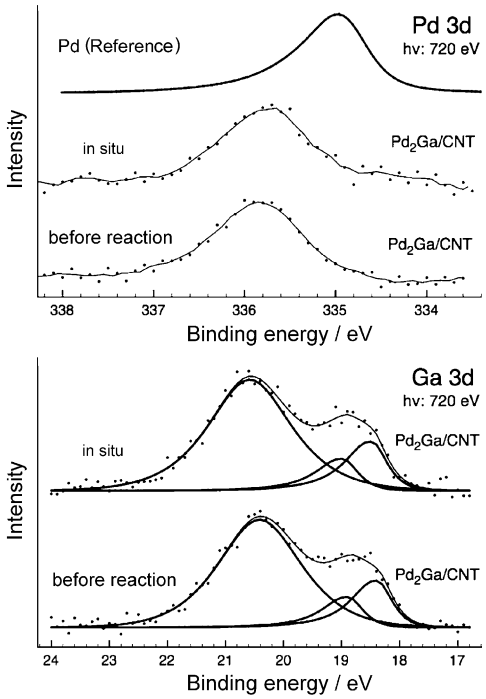

Figure 4. In situ XPS analyses of Pd 3d and Ga 3d regions for the Pd_2Ga/CNT before reaction and during hydrogenation of acetylene.

carbon nanotubes (Figure 5a). Pd_2Ga/CNT was then heated in the reactant gas mixture (C_2H_2 and H_2). In situ XRD studies showed no detectable peak shift or pattern changes under applied conditions (Figure 5a).

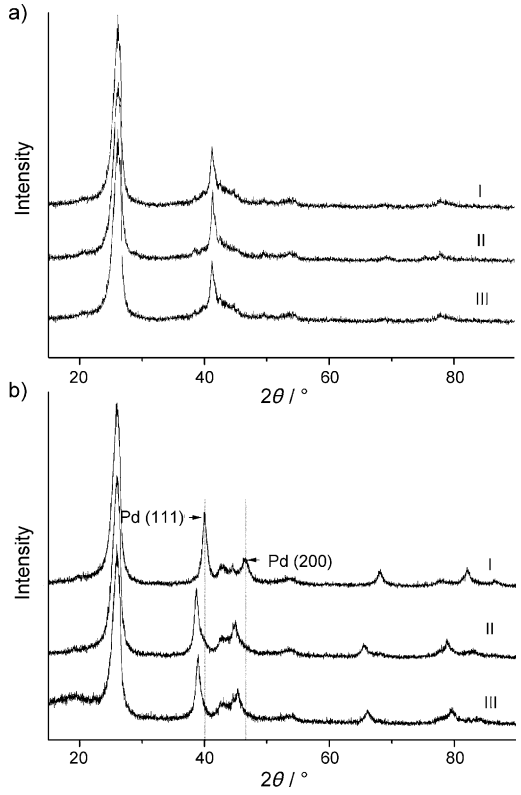

Figure 5. In situ XRD investigations with a) Pd_2Ga/CNT and b) Pd/CNT: fresh sample (I), recorded under H_2 (II), recorded under reaction conditions (III).

It was reported that carbon species modify the Pd catalyst in alkyne selective hydrogenation by forming a subsurface PdC_x.[35] Hydrogen, as another reactant, often changes the structure of Pd catalyst and affects hydrogenation by forming active but unselective β-hydride.[36] Therefore, to better understand the structural stability of Pd_2Ga/CNTs, Pd supported on CNTs (Pd/CNT) was prepared as a reference sample, and an equal amount of palladium was deposited on CNTs using the same method as Pd_2Ga synthesis. For Pd/CNT recorded in H_2 (Figure 5b), the XRD pattern of Pd(111) exhibited a shift to 2θ angle 38.8°,which corresponds to a lattice constant $a = 4.02$ Å and confirms the β-hydride formation.[37] Switching on the reaction led to a shift to 2θ angle 39°, which indicates an expansion of palladium crystalline constant caused by PdC_x formation.[38] (Figure 5b) Microscopy observations for reacted Pd/CNT exhibit a heavy carbon deposition on Pd and CNT surfaces (Supporting Information, Figure S1a, S2a).

In contrast to reference Pd/CNT, in situ XRD investigations on Pd_2Ga/CNT showed that β-hydride and PdC_x were suppressed on Pd_2Ga/CNT, which is in line with XPS observations. Moreover, microscopy studies for reacted Pd_2Ga/CNT displayed obvious differences in morphology compared with reference Pd/CNT. No clear appearance of carbon deposition was observed and Pd_2Ga particles remained nanoscale both in STEM and HRTEM modes (Supporting Information, Figure S1b, S2b), which indicate that adding Ga and forming covalent interactions restrict Pd particle sintering and suppress carbonaceous depositions. Furthermore, STEM-EDX line profiles showed that Pd and Ga compositions remained constant on the Pd_2Ga nanoparticles before and after reaction (Supporting Information, Figure S3). Microscopy studies, together with in situ XRD investigations, reveal a structural stability for Pd_2Ga intermetallics supported on CNTs.

Catalysis studies of Pd_2Ga/CNT (0.24 mg) were carried out and compared with $Pd_{20}Ag_{80}$ (alloy catalyst as a reference, 200 mg). Figure 6a reveals that Pd_2Ga/CNT exhibits a long-term stability at conversion of 90% throughout 20 h on stream. An activity of 856.8 $g_{C_2H_2}\,g_{Pd}^{-1}\,h^{-1}$ was obtained, while selectivity remained at 58.1% at 20 h. In the case of the $Pd_{20}Ag_{80}$ catalyst, a selectivity of 49% and activity of 0.2 $g_{C_2H_2}\,g_{Pd}^{-1}\,h^{-1}$ was obtained (Figure 6b). While the obtained selectivity is 9% higher, the activity of Pd_2Ga/CNT is several orders of magnitude higher than that of $Pd_{20}Ag_{80}$.

In summary, distinct from conventional annealing methods to establish covalent interactions in intermetallics, we have presented an impregnation method to synthesize nanocrystalline Pd_2Ga intermetallics onto CNTs. Oxidized vacancies and localized double bonds on CNTs inhibit sintering and loss of the Pd_2Ga nanoparticles during reactions. Nanocrystalline intermetallics have abundant low coordination sites (edge, stepped, and kink) on surfaces, and thereby lead to a high activity. The surface and structure of obtained Pd_2Ga nanoparticles are thermally stable under reaction conditions. Establishing covalent interactions within nanocrystalline

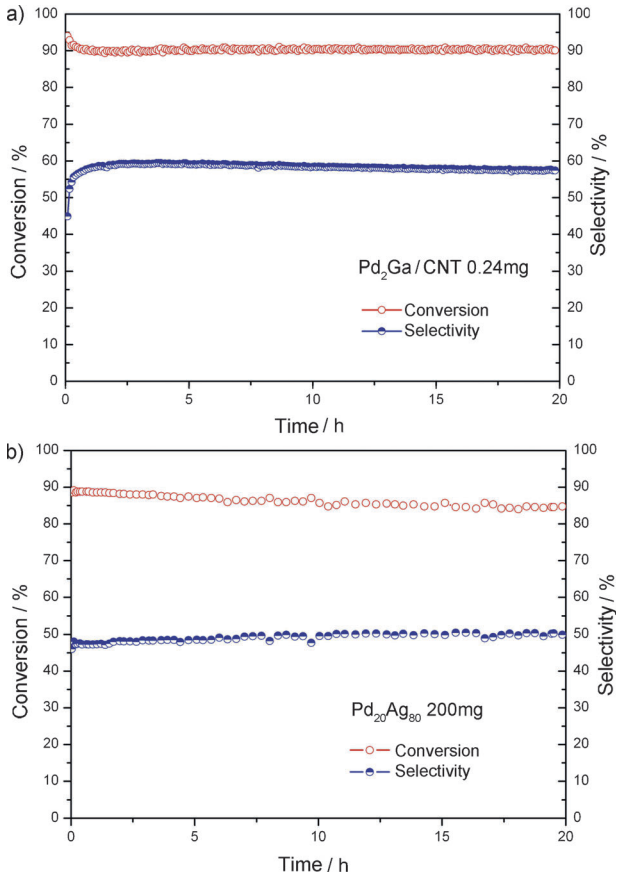

Figure 6. Conversion and selectivity during acetylene hydrogenation on a) Pd_2Ga/CNT and b) $Pd_{20}Ag_{80}$, measured by isothermal experiments at 200 °C.

intermetallics forms a high barrier for subsurface chemistry and reduces large active ensembles, which can be reflected in the improved selectivity. The absence of structural dynamics under reaction conditions makes nanocrystalline Pd_2Ga ideal targets for realistic model studies. The approach of nanosizing intermetallics onto CNTs while obtaining good control of crystallite size may be applicable for synthesizing and supporting other nanocrystalline intermetallic compounds.

Experimental Section

PR24-LHT carbon nanotubes were purchased from Pyrograf Products Inc. (Ohio, USA). Concentrated nitric acid (70%, Sigma–Aldrich) was used to functionalize CNTs at 110 °C for 4 h. Pd_2Ga/CNT was prepared by the following route: palladium nitrate (34.1 mg, ca. 40% Pd, Roth) and gallium nitrate hydrate (53.5 mg, 99.9%, Alfa) were dissolved in ethanol (80 mL). functionalized CNTs (300 mg) were then mixed into the solution. Ultrasonication was carried out for one hour and followed by evaporation at room temperature. The sample was then collected and calcinated in air at 250 °C. Reduction was conducted in 25% H_2 mixed with He in a total flow of 100 mL min^{-1} at 550 °C. Pd/CNT was prepared in the same route, and the same amount of palladium nitrate (ca. 40% Pd, Roth) and CNTs were used. The alloy referred to as $Pd_{20}Ag_{80}$ in the text was prepared by melting 1.2047 g Ag (99.995% ChemPur) and 0.3035 g Pd (99.95% ChemPur) three times in an arc melter under argon. Subsequently, the regulus obtained was enclosed in an evacuated quartz glass ampule and annealed at 800 °C for six days. After the heat treatment, the regulus was filed and the phase purity of the obtained Pd-Ag alloy (Cu type of structure, $Fm\bar{3}m$, $a = 4.0456(6)$ Å) was confirmed by X-ray powder diffraction (STOE STADI P diffractometer, $Cu_{K\alpha_1}$ radiation, $\lambda = 1.540598$ Å, curved Ge monochromator).

Catalysis measurements were conducted in a feed (30 mL min^{-1}) of 0.5% C_2H_2, 5% H_2 (99.999%) and 50% C_2H_4 (99.95%) in helium (99.999%). For more experimental details, see the Supporting Information.

Received: December 19, 2010
Revised: April 5, 2011
Published online: June 28, 2011

Keywords: carbon nanotubes · electron microscopy · hydrogenation · intermetallic phases · nanostructuring

[1] C. Roychowdhury, F. Matsumoto, P. F. Mutolo, H. D. Abruña, F. J. DiSalvo, *Chem. Mater.* **2005**, *17*, 5871.
[2] C. Roychowdhury, *Chem. Mater.* **2006**, *18*, 3365.
[3] F. Matsumoto, C. Roychowdhury, F. J. DiSalvo, H. D. Abruña, *J. Electrochem. Soc.* **2008**, *155*, B148.
[4] J. C. Bauer, X. Chen, Q. Liu, T.-H. Phan, R. E. Schaak, *J. Mater. Chem.* **2008**, *18*, 275.
[5] E. Casado-Rivera, *ChemPhysChem* **2003**, *4*, 193.
[6] E. Casado-Rivera, *J. Am. Chem. Soc.* **2004**, *126*, 4043.
[7] C. Rice, S. Ha, R. I. Masel, A. Wieckowski, *J. Power Sources* **2003**, *115*, 229.
[8] X. Ji, K. T. Lee, R. Holden, L. Zhang, J. Zhang, G. A. Botton, M. Couillard, L. F. Nazar, *Nat. Chem.* **2010**, *2*, 286.
[9] S. Park, Y. Xie, M. J. Weaver, *Langmuir* **2002**, *18*, 5792.
[10] J. D. Lović, A. V. Tripković, S. Lj. Gojković, K. Đ. Popović, D. V. Tripković, P. Olszewski, A. Kowal, *J. Electroanal. Chem.* **2005**, *581*, 294.
[11] K. Kovnir, M. Armbrüster, D. Teschner, T. V. Venkov, F. C. Jentoft, A. Knop-Gericke, Yu. Grin, R. Schlögl, *Sci. Technol. Adv. Mater.* **2007**, *8*, 420.
[12] J. Osswald, R. Giedigkeit, R. E. Jentoft, M. Armbrüster, F. Girgsdies, K. Kovnir, T. Ressler, Yu. Grin, R. Schlögl, *J. Catal.* **2008**, *258*, 210.
[13] J. Osswald, K. Kovnir, M. Armbrüster, R. Giedigkeit, R. E. Jentoft, U. Wild, Yu. Grin, R. Schlögl, *J. Catal.* **2008**, *258*, 219.
[14] K. Kovnir, M. Armbrüster, D. Teschner, T. V. Venkov, L. Szentmiklósi, F. C. Jentoft, A. Knop-Gericke, Yu. Grin, R. Schlögl, *Surf. Sci.* **2009**, *603*, 1784.
[15] K. Kovnir, J. Osswald, M. Armbrüster, D. Teschner, G. Weinberg, U. Wild, A. Knop-Gericke, T. Ressler, Yu. Grin, R. Schlögl, *J. Catal.* **2009**, *264*, 93.
[16] R.Giedigkeit, Intermetallische Verbindungen im System Yb-Pd-Ga. Diploma Thesis, Technische Universität Darmstadt, **1998**.
[17] M. Armbrüster, K. Kovnir, M. Behrens, D. Teschner, Yu. Grin, R. Schlögl, *J. Am. Chem. Soc.* **2010**, *132*, 14745.
[18] G. Rupprechter, M. Morkel, H.-J. Freund, R. Hirschl, *Surf. Sci.* **2004**, *554*, 43.
[19] D. Mei, M. Neurock, C. M. Smith, *J. Catal.* **2009**, *268*, 181.
[20] S. Iijima, *Nature* **1991**, *354*, 5.
[21] T. W. Ebbesen, *Phys. Today* **1996**, *49*, 26.
[22] M. Inagaki, L. R. Radovic, *Carbon* **2002**, *40*, 2279.
[23] J. M. Carlsson, F. Hanke, S. Linic, M. Scheffler, *Phys. Rev. Lett.* **2009**, *102*, 166104.
[24] J. M. Carlsson, M. Scheffler, *Phys. Rev. Lett.* **2006**, *96*, 046806.
[25] E. P. J. Parrott, J. A. Zeitler, J. McGregor, S. P. Oei, H. E. Unalan, S. C. Tan, W. I. Milne, J. P. Tessonnier, R. Schlögl, L. F. Gladden, *J. Phys. Chem. C* **2009**, *113*, 10554.
[26] J. P. Tessonnier, D. Rosenthal, F. Girgsdies, J. Amadou, D. Begin, D. Pham-Huu, D. S. Su, R. Schlögl, *Chem. Commun.* **2009**, 7158.

[27] G. Wulff, *Z. Kristallogr.* **1901**, *34*, 449.
[28] P. L. Hansen, J. B. Wagner, S. Helveg, J. R. Rostrup-Nielsen, B. S. Clausen, H. Topsoe, *Science* **2002**, *295*, 2053.
[29] K. Schubert, H. L. Lukas, H. G. Meissner, S. Bhan, *Z. Metall.* **1959**, *50*, 534.
[30] K. Kovnir, M. Schmidt, C. Waurisch, M. Armbrüster, Yu. Grin, *Z. Kristallogr. New Cryst. Struct.* **2008**, *223*, 7.
[31] D. Teschner, A. Pestryakov, E. Kleimenov, M. Havecker, H. Bluhm, H. Sauer, A. Knop-Gericke, R. Schlögl, *J. Catal.* **2005**, *230*, 186.
[32] D. Teschner, A. Pestryakov, E. Kleimenov, M. Havecker, H. Bluhm, H. Sauer, A. Knop-Gericke, R. Schlögl, *J. Catal.* **2005**, *230*, 195.
[33] F. Scharmann, G. Cherkashinin, V. Breternitz, C. Knedlik, G. Hartung, T. Weber, J. A. Schaefer, *Surf. Interface Anal.* **2004**, *36*, 981.
[34] C. C. Surdu-Bob, S. Saied, J. Sullivan, *Appl. Surf. Sci.* **2001**, *183*, 126.
[35] D. Teschner, J. Borsodi, A. Wootsch, Z. Révay, M. Hävecker, A. Knop Gericke, S. D. Jackson, R. Schlögl, *Science* **2008**, *320*, 86.
[36] M. García-Mota, B. Bridier, J. Pérez-Ramírez, N. López, *J. Catal.* **2010**, *273*, 92.
[37] J. Stachurski, A. Frackiewicz, *J. Less-Common Met.* **1985**, *108*, 249.
[38] S. B. Ziemecki, G. A. Jones, D. G. Swartzfager, R. L. Harlow, *J. Am. Chem. Soc.* **1985**, *107*, 4547.

